Available online at www.sciencedirect.com
SCIENCE DIRECT®
Journal of Nuclear Materials 335 (2004) 433–442
journal of nuclear materials
www.elsevier.com/locate/jnucmat

Crystal structure and grain size of Zr oxide characterized by synchrotron radiation microdiffraction

Jeong-Yong Park *, Hyun-Gil Kim, Yong Hwan Jeong, Youn-Ho Jung

Zirconium Fuel Cladding Team, Korea Atomic Energy Research Institute, 150 Doekjin-dong, Yuseong-gu, Daejeon 305-353, Korea

Received 12 April 2004; accepted 22 July 2004

Abstract

Zirconium oxides formed on Zirclaoy-4 and Zr–1.5Nb (in wt%) were characterized by the microbeam X-ray diffraction using a synchrotron radiation. The phase fraction and the grain size were determined as a function of the position in the oxide. It was found that Zr–1.5Nb showed the better corrosion resistance than Zircaloy-4 in 360 °C pure water although the tetragonal phase was more stabilized to a further distance from the metal/oxide interface in the oxide of Zircaloy-4. The calculation of the grain size revealed that the oxide of the Zr–1.5Nb had larger grains than that of Zircaloy-4 with the tetragonal phase being smaller than the monoclinic one. It seems reasonable to suppose that the superior corrosion resistance of Zr–1.5Nb was attributed to the lager grain size of the oxide in which the oxygen diffusion is expected to be lowered when compared to the smaller grain size of the oxide on Zircaloy-4.

PACS: 81.65.K; 81.65.M; 29.20.L

1. Introduction

Fuel claddings are considered to be the most important part of a nuclear fuel assembly because their performance is directly related to the safety and the economic operation of nuclear power plants. Zr alloys, e.g., Zircaloy-4, have been used as fuel cladding tubes in pressurized water-cooled reactors (PWRs) due to their low thermal neutron cross-section and high corrosion resistance in a coolant condition. Since the corrosion of fuel claddings is one of the most critical issues in developing the high burn-up fuel, a number of efforts have been focused on improving the corrosion resistance of the Zr alloys through a further optimization of the existing commercial alloys [1] and the development of advanced alloys such as ZIRLO [2] and M5 [3].

It has been reported that the corrosion resistance of Zr alloys is highly affected by the metallurgical parameters including the alloy composition [4], intermetallic precipitates [5] and manufacturing process [6], which influence the oxide characteristics dominating the corrosion kinetics. Among a variety of metallurgical parameters that are well linked to the corrosion kinetics of Zr alloys, the Nb addition is known to be beneficial to the corrosion resistance of Zr alloys when the Nb content is properly controlled and the heat treatment is performed below the transformation temperature from α to β phase [2,3]. It is worthy to note that the relationship between the precipitate characteristics and the corrosion

* Corresponding author. Tel.: +82 42 868 8911; fax: +82 42 862 0432.
E-mail address: parkjy@kaeri.re.kr (J.-Y. Park).

0022-3115/$ - see front matter © 2004 Elsevier B.V. All rights reserved.
doi:10.1016/j.jnucmat.2004.07.051

resistance of the Nb-containing Zr alloys [3] is different from that proposed for Zircaloy-4 [7].

The mechanistic understanding for the corrosion of Zr alloys can be established by characterizing the oxide precisely. Crystal structure and grain morphology are major parameters that have been extensively investigated to correlate the oxide characteristics to the corrosion kinetics of Zr alloys. A number of investigations revealed that the crystal structure [8] and grain morphology [9,10] could be closely related to the corrosion kinetics of Zr alloys although many controversies still remain.

In order to enhance the understanding of the relationship between the oxide characteristics and the corrosion kinetics of Zr alloys, the local properties of the oxide are required rather than the bulk properties. Although many researchers have characterized the Zr oxide using a number of different methods, most of their results, however, provided only the bulk properties of the oxide, which could not clarify the relationship between the oxide characteristics and the corrosion kinetics. Recently, the characterization using a synchrotron radiation [11–13] has been considered to be one of the most promising technologies to assess the characteristics of the Zr oxide on a microscale.

The purpose of this investigation is to characterize the Zr oxide as a function of the position from the metal/oxide interface to the outer oxide by use of the X-ray microbeam obtained from a synchrotron radiation source. Zr–1.5Nb (in wt%) alloy and Zircaloy-4 tube were selected to examine the change of the corrosion characteristics with the alloying elements. Crystal structure, phase distribution and grain size of the Zr oxide were determined from the microbeam X-ray diffraction experiment and the relationship between the oxide characteristics and the corrosion kinetics was discussed.

2. Experimental methods

2.1. Alloys

Zr–1.5Nb alloy was selected to investigate the corrosion behavior and the oxide characteristics with the reference alloy of Zircaloy-4 which has been used as commercial nuclear fuel claddings in PWRs. We have investigated the change of the corrosion behavior with the alloying elements through the oxide characterization.

Zr–1.5Nb alloy was manufactured to sheet-type specimens in the laboratory whereas the Zircaloy-4 tube was used in an as-received state. A button ingot of approximately 200 g with a target composition of Zr–1.5wt%Nb was prepared by arc melting under an argon atmosphere and remelted at least five times to promote the homogeneity of the as-cast structure. The arc-melted ingot was water-quenched after a β-solution treatment at 1020 °C for 30 min in a vacuum furnace, hot-rolled after preheating at 610 °C for 10 min, and cold-rolled three times to a final thickness of 1 mm. The cold-rolled sheets were intermediate-annealed at 570 °C for 3 h between each cold rolling. The final cold-rolled sheet was subjected to the water-quenching and annealed at 570 °C for 500 h to obtain the fully-recrystallized structure.

2.2. Microstructure observation

The microstructures of the alloys were examined using a transmission electron microscope (TEM) equipped with an energy dispersive X-ray spectroscope (EDS). Specimens for the TEM observation were prepared by twin-jet polishing with a solution of 10 vol.% $HClO_3$ and 90 vol.% C_2H_5OH after a mechanical thinning to about 70 μm. The microstructure observation was concentrated on the characteristics of the precipitates since it is well known that the corrosion resistance of the Zr alloys is highly dependant on the characteristics of the precipitates. The selected area diffraction patterns (SADP) were obtained to determine the crystal structure of the precipitates, and the microchemical analyses on the precipitates were conducted using EDS.

2.3. Corrosion test

Zircaloy-4 tube, 9.5 mm in outer diameter and 0.6 mm in wall thickness, was cut to the length of 20 mm for the corrosion test. Corrosion test specimens of Zr–1.5Nb, 15 mm by 20 mm by 1 mm in size, were cut from the fully-recrystallized sheet and mechanically ground up to 1200 grit SiC paper. And then the specimens for the corrosion test were pickled in a solution of 5 vol.% HF, 45 vol.% HNO_3 and 50 vol.% H_2O. The corrosion tests were conducted in 360 °C pure water under a saturation pressure of 18.5 MPa according to ASTM G2-88. The corrosion behavior of the alloys was evaluated by measuring the weight gain with the exposure time. The corrosion test was conducted for 300 days using four samples per each alloy. After 150 days of the corrosion test, one of the four corroded samples for each alloy was taken out to characterize the oxide.

2.4. Oxide characterization by synchrotron radiation microdiffraction

The oxide characterization was carried out by the X-ray diffraction method using a synchrotron radiation. The specimens for the diffraction experiment were prepared by cross-sectioning the corroded samples followed by a mechanical polishing of the cross-section up to 2000 grit SiC paper. Fig. 1 shows the experimental setup of the microdiffraction using a synchrotron radiation. The diffraction experiment was performed at the 1B2

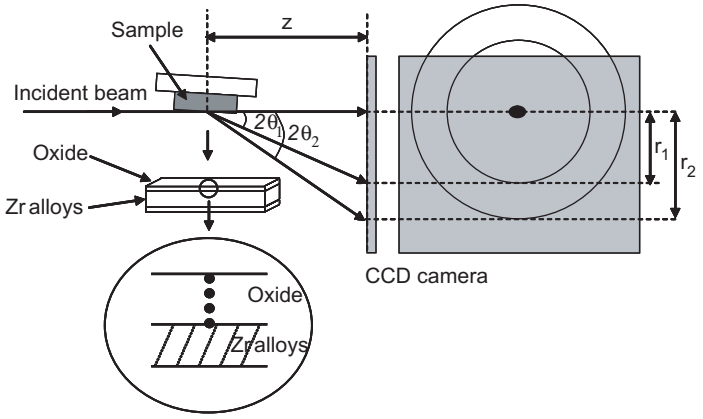

Fig. 1. Schematic drawing showing the experimental setup for the microbeam X-ray diffraction using synchrotron radiation.

bending magnet beamline of the Pohang light source (PLS) in Korea. The beam energy of 12 keV, which corresponds to a wavelength of 0.1033167 nm, was used to obtain the diffraction pattern of interest in the diffraction geometry depicted in Fig. 1.

The size of the incident beam on the sample was 10 μm in the horizontal direction by 1 μm in the vertical direction to the metal/oxide interface. Such a beam dimension has an advantage that it enables us to obtain a high spatial resolution in a direction normal to the metal/oxide interface and to analyze as large a volume of oxide as possible at a certain position from the interface. The microbeam X-ray is incident on the region of interest in the oxide and the diffracted intensity in the form of a ring pattern is detected by a CCD camera. Upon varying the position of the incident beam, it was possible to assess the crystal structure of the oxide as a function of the position from the metal/oxide interface to the outer oxide.

3. Results and discussion

3.1. Microstructures

Fig. 2 shows the microstructures of the Zircaloy-4 and Zr–1.5Nb used in this study. Since the as-received Zircaloy-4 was subjected to the final annealing of 470 °C, it shows a typical stress-relived microstructure in which a great number of the dislocations produced by the prior cold rolling were tangled up with each other. The recrystallized grains were also found, which were surrounded by the tangled dislocation and they contained precipitates which were identified as $Zr(Fe,Cr)_2$ in the previous investigation [7]. It has been well known that the characteristics of $Zr(Fe,Cr)_2$ precipitate are closely related to the corrosion behavior of Zircaloy-4; the corrosion resistance of Zircaloy-4 was improved when the average particle size of the $Zr(Fe,Cr)_2$ precipitate was more than 100 nm [7].

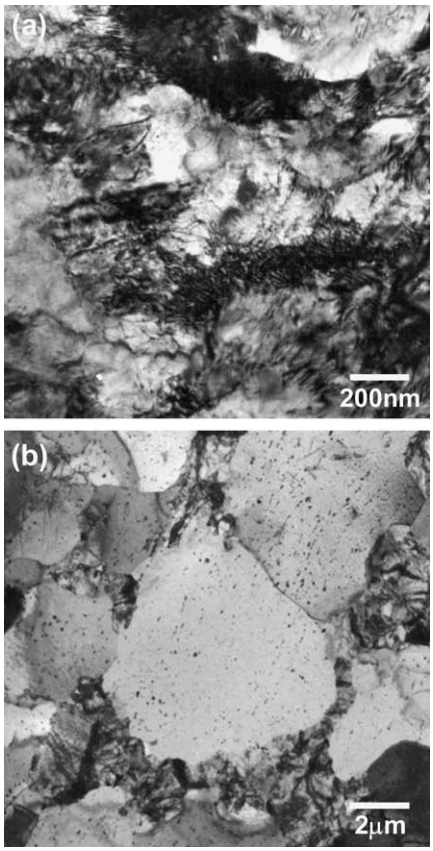

Fig. 2. Transmission electron micrographs of (a) the stress-relieved Zircaloy-4 tube and (b) Zr–1.5wt%Nb alloy annealed at 570 °C for 500 h.

Zr–1.5Nb shows the fully-recrystallized microstructure in which a lot of precipitates formed in the

recrystallized grain as well as the grain boundary since it was annealed at 570 °C for 500 h. The authors' previous investigation [13] revealed that two types of precipitates existed in the Zr–1.5Nb alloys. Most of the precipitates, whose average size was less than approximately 80 nm, were identified as β_{Nb} which had a bcc crystal structure and contained more than 70 at.% Nb. The other type of precipitates were identified as $Zr(Nb,Fe)_2$ with a hcp crystal structure and their average size was larger than β_{Nb}. The corrosion resistance of the Nb-containing Zr alloys has been reported to improve when the small precipitates are distributed homogeneously over the recrystallized grains by a heat treatment at a low temperature [14], which is contrary to Zircaloy-4 [7].

3.2. Corrosion behavior

Fig. 3 shows the corrosion behavior of the alloys in an autoclave of 360 °C pure water up to 300 days. Zr–1.5Nb showed a better corrosion resistance than Zircaloy-4 although its corrosion weight gain was larger than Zircaloy-4 at an early stage of corrosion before 150 days. Corrosion rate of Zircaloy-4 was accelerated after 90 days and changed periodically while Zr–1.5Nb did not show any transition behavior in the corrosion rate and maintained a lower corrosion rate up to 300 days.

The weight gains of the two alloys were almost same as each other at about 60 mg/dm^2 at 150 days of the corrosion test, which provided the same oxide thickness of about 4 μm for each alloy. Therefore, oxide characterization was performed on the oxide formed at 150 days for each alloy. It might be a relatively thin oxide that maintained the sound protectiveness. However, such a thin oxide formed at an early stage of corrosion would provide more decisive information on the corrosion behavior hereafter rather than the thicker oxide formed at a later stage. This is the reason why the relatively thin oxides with the same thickness were selected for the characterization in this investigation.

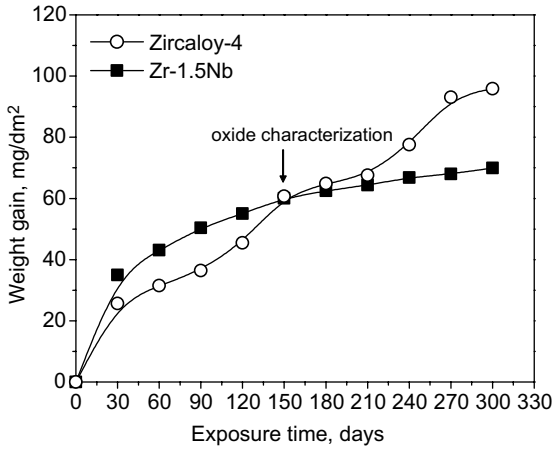

Fig. 3. Corrosion behavior of Zircaloy-4 and Zr–1.5wt%Nb in pure water at 360 °C.

3.3. Phase distribution in oxides

The oxides formed at 150 days of the corrosion test for Zricaloy-4 and Zr–1.5Nb were characterized as a function of the distance from the metal/oxide interface using the synchrotron radiation microdiffraction method described in Section 2.4. Fig. 4 shows the microbeam X-ray diffraction patterns from the oxide formed on the Zircaloy-4 corroded to a weight gain of about 60 mg/dm^2. The ring patterns were shown to be similar irrespective of the position from which the diffracted beams were produced though the diffracted intensity from the interface region was stronger than that from the outer oxide. From the diffraction patterns and the experimental geometry shown in Fig. 1, the phases with the diffracted planes which produced the diffracted intensity were identified using the following equation:

$$\lambda = 2d\sin(0.5\tan^{-1}(r/z)), \quad (1)$$

where λ is the wavelength of the incident beam, d is the spacing of the diffracted plane, r is the radius of the ring pattern and z is the distance from the diffracted region to the CCD camera.

After the indexing of the ring patterns, the oxide was found to consist of the tetragonal and monoclinic phase as reported in the previous study [8]. Even in the same ring pattern, the intensity was different depending on the position, which suggests that the texture was developed in the oxide.

Fig. 5 shows the diffracted intensity as a function of the two-theta for the oxide formed on the Zircaloy-4. The diffracted intensity in Fig. 5 was obtained by integrating the intensity of the ring patterns of interest shown in Fig. 4, which corresponds to the tetragonal and monoclinic phase at a certain position in the oxide. The diffracted intensity was enhanced when the diffracted volume was changed from the region of the outer oxide to the interface region with the incident beam moving from the outer oxide to the interface. In the region of the metal/oxide interface, the diffracted intensity from the Zr metal matrix was increased and the intensity corresponding to the tetragonal phase was also enhanced, which implies that the fraction of the tetragonal phase is higher at the interface region than the outer region in the oxide formed on the Zircaloy-4.

Fig. 6 shows the microbeam X-ray diffraction patterns from the oxide formed on the Zr–1.5Nb corroded to a weight gain of about 60 mg/dm^2. The diffraction patterns were similar to that of the Zircaloy-4 shown in Fig. 4 and were shown to be a little stronger near the interface region compared to the outer region in the oxide. By indexing the ring patterns using Eq. (1),

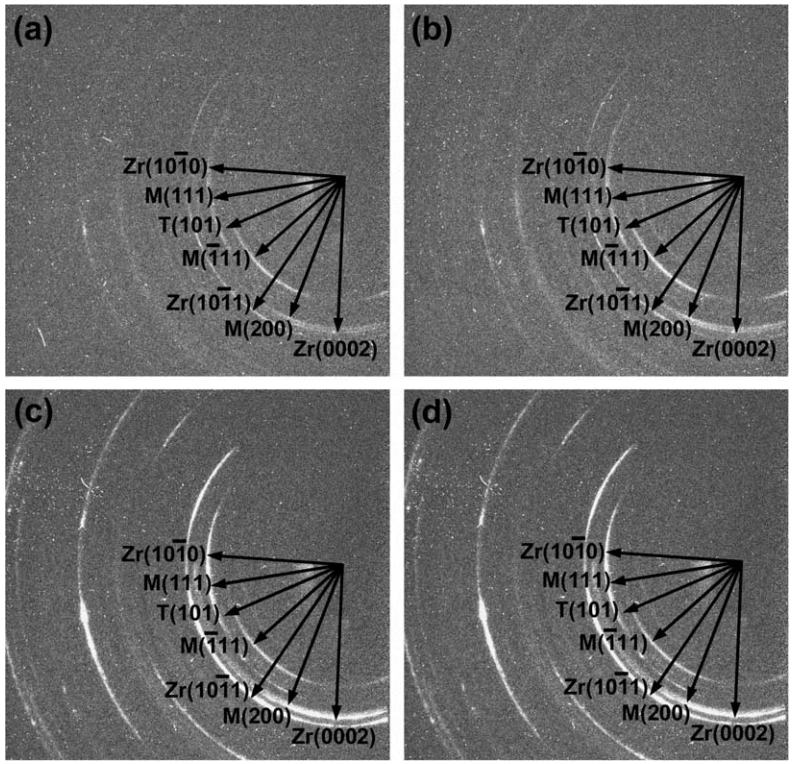

Fig. 4. Microbeam X-ray diffraction patterns from the oxide formed on the Zircaloy-4 corroded to a weight gain of 60 mg/dm^2: (a) outer oxide, (b) upper inner oxide, (c) lower inner oxide and (d) metal/oxide interface.

it was found that the oxide formed on the Zr–1.5Nb was a mixture of the tetragonal and monoclinic phase as revealed in the Zricaloy-4.

Fig. 7 shows the diffracted intensity plotted against the two-theta angle for the oxide formed on the Zr–1.5Nb. The diffracted intensity peaks corresponding to the tetragonal and monoclinic phase were shown to exist and a strong intensity for the Zr matrix was also found especially in the interface region. The oxide on the Zr–1.5Nb consists of the tetragonal and monoclinic phase though the relative intensity of the phases was different from that of the Zircaloy-4 shown in Fig. 5. It was worthy of note that the (1 0 1) peak of the tetragonal phase became stronger in the region of the interface both in the Zircaloy-4 and Zr–1.5Nb. This result manifested that the tetragonal phase could be more easily stabilized in the interface as compared to the outer surface region in the oxide irrespective of alloy compositions.

The phase distribution in the oxide was examined quantitatively. After indexing each peak on the diffracted intensity plotted against the two-theta angle shown in Figs. 5 and 7, the peak fitting process was performed on the peak corresponding to the tetragonal and monoclinic phase to quantify precisely the amount of the tetragonal and monoclinic phase present in the oxide. The fraction of the tetragonal phase was calculated using the following equation which was proposed to calculate the phase fraction of the ZrO_2 powder [15].

$$F_t = I_{t(1\,0\,1)}/(I_{m(1\,1\,1)} + I_{t(1\,0\,1)} + I_{m(\bar{1}\,1\,1)}), \quad (2)$$

where the $I_{t(1\,0\,1)}$ is the integrated intensity for the (1 0 1) peak of the tetragonal phase and $I_{m(\bar{1}\,1\,1)}$ and $I_{m(1\,1\,1)}$ are the integrated intensities for the ($\bar{1}$ 1 1) peak and the (1 1 1) peak of the monoclinic phase, respectively.

Fig. 8 shows the calculated fraction of the tetragonal phase as a function of the distance from the metal/oxide interface in the oxide formed on the Zircaloy-4 and Zr–1.5Nb. As shown in Fig. 8, the fraction of the tetragonal phase in the oxide ranged from 5% to 15% over the entire oxide with a decreasing tendency from the metal/oxide interface to the outer surface. It was also found that the fraction of the tetragonal phase in both alloys was almost the same at the interface and decreased when apart from the interface. The tetragonal fraction of Zircaloy-4 maintained its higher value at a further distance from the interface than that of Zr–1.5Nb.

Since it is widely known that the oxide formed on the Zr alloys has a texture structure, texture correction should be performed to obtain the precise calculation of the phase fraction. Yilmazbayhan et al. [11] analyzed the crystal structures of the oxides formed on the four different zirconium alloys (Zircaloy-4, ZIRLO,

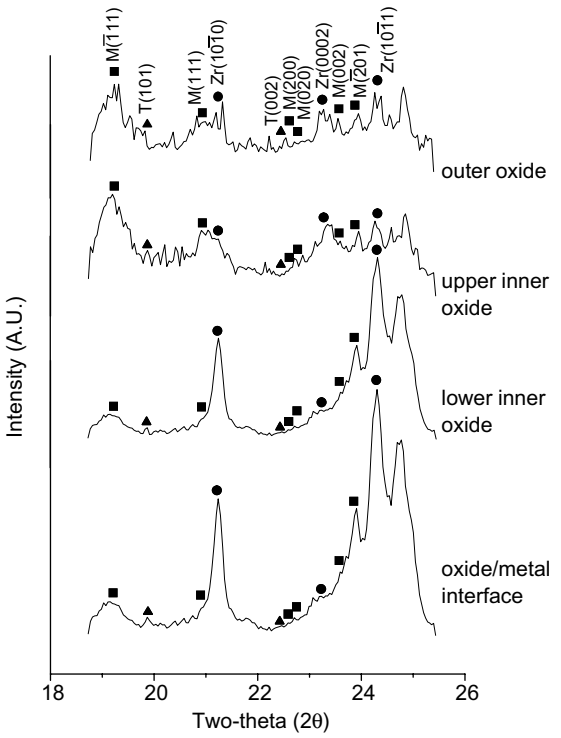

Fig. 5. Diffracted intensity plotted against the two-theta angle for the oxide formed on Zircaloy-4.

Zr–2.5%Nb and Zr–2.5%Nb–0.5%Cu) as a function of position in the oxide by a synchrotron radiation. Though the texture correction was performed to calculate the fraction of the tetragonal phase, the same texture correction factor was applied irrespective of the alloy composition by the assumption that the texture does not change greatly with oxide thickness and with alloy type. The same assumption was applied to our investigation because what was emphasized in the phase calculation was the difference of the phase fraction gradient between Zircaloy-4 and Zr–1.5Nb. Although it is difficult to calculate the absolute value of the tetragonal volume fraction in the oxide from the result obtained in this investigation, it could be clarified that the tetragonal phase fraction is a maximum near the metal/oxide interface and decreased when apart from the interface both in Zircaloy-4 and Zr–1.5Nb.

In general, the oxide of the Zr alloys was reported to consist of two layers according to the degree of the porosity. Dense oxide was formed in the interface region while the oxide in the outer surface region could be characterized as porous [16]. In addition, the outer oxide consisted mainly of a monoclinic structure whereas the tetragonal and monoclinic structures were mixed up in the interface region [8]. It was known that the corrosion behavior of the Zr alloys was controlled by the dense oxide layer near the interface. And the corrosion resistance of the Zr alloys was improved when the fraction of the tetragonal structure increased in the dense oxide layer near the interface [8]. The tetragonal phase in the Zr oxide is stable at temperatures above 1150 °C, but it can be stabilized at lower temperatures in the presence of high compressive stresses. It was proposed that the high compressive stresses developed during the oxidation due to the high Pilling–Bedworth ratio (1.56 for Zr) were responsible for the stabilization of the tetragonal phase [8,17,18].

Another reason why the tetragonal phase is stabilized in the oxide of the Zr alloys originates from grain size of the oxide near the interface. It has been reported that the tetragonal phase is more easily stabilized when the grain size of the oxide near the interface is small [19–21]. This result is consistent with the result that the monoclinic phase was more easily stabilized compared to the tetragonal structure when the surface energy is increased [22]. However, the grain size cannot fully explain the phenomena that the tetragonal structure which has been formed in the interface region disappeared when the metal matrix was removed to observe the oxide.

In addition, the stability of the tetragonal phase can be affected by alloying elements. It was reported that Fe and Sn enhanced the stability of the tetragonal phase near the $Zr(Fe,Cr)_2$ precipitate [23]. On the contrary, Nb was reported to decrease the stability of the tetragonal phase in the Zr–1.0wt%Nb alloys [24]. However, it is thought that the content of the alloying elements is too small in the oxide to affect the stability of the crystal structure. It is therefore suggested that the effect of alloying elements on the stability of the crystal structure in the oxide was not dominant. This seems to be one of the reasons why the fraction of the tetragonal phase at the interface was the same in both alloys of this investigation even though the corrosion behavior was different depending on the alloy compositions.

Godlewski et al. [25] have measured the stress gradient in the Zr oxide using a Raman spectroscopy and correlated the stress build-up with the tetragonal phase stability. The measured compressive stress distribution was well correlated to the tetragonal phase stability. The tetragonal phase fraction was higher in the metal/oxide interface where the compressive stress was determined to be higher. When the compressive stress decreased to a certain level in the outer part of the oxide, the tetragonal phase was destabilized and transformed into the monoclinic phase. The compressive stress determined using a Raman spectroscopy ranged from 800 MPa to 1.5 GPa which is lower than the theoretically computed value by Parise et al. [26]. The calculated compressive hoop stress during Zircaloy-4 corrosion was evaluated to be about 2 GPa at the metal/oxide interface along with a very weak radial stress and weak tensile stress.

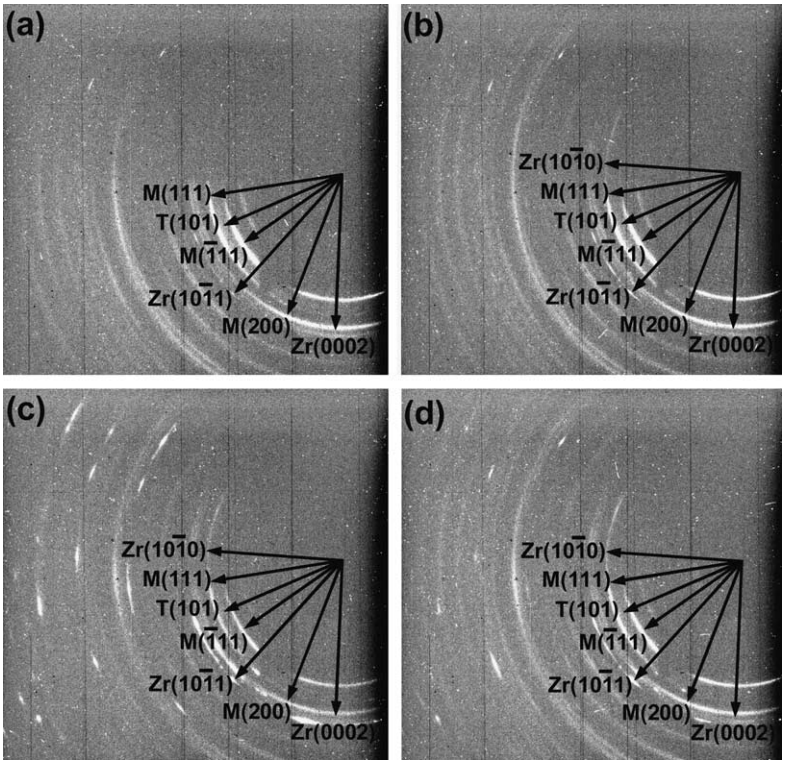

Fig. 6. Microbeam X-ray diffraction patterns from the oxide formed on the Zr–1.5wt%Nb corroded to a weight gain of 60 mg/dm^2: (a) outer oxide, (b) upper inner oxide, (c) lower inner oxide and (d) metal/oxide interface.

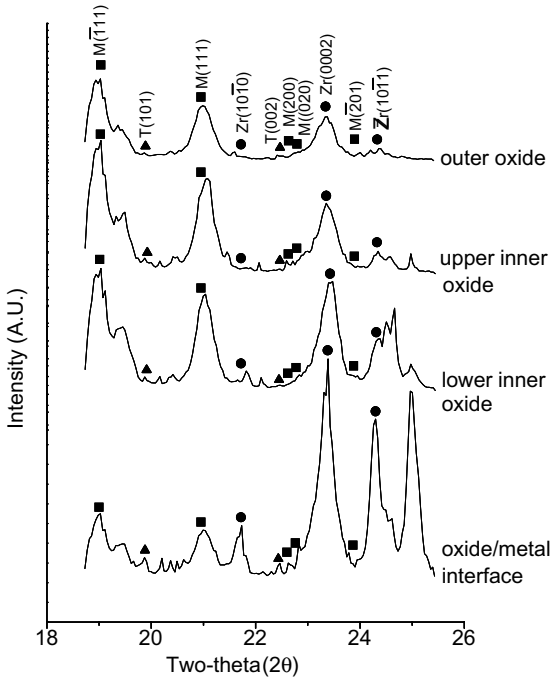

Fig. 7. Diffracted intensity plotted against the two-theta angle for the oxide formed on Zr–1.5wt%Nb.

It was found that the tetragonal phase in the oxide of Zircaloy-4 was more stable as a whole, as shown in Fig. 8. This might suggest that stress build-up in the oxide of Zircaloy-4 is higher as compared to Zr–1.5Nb. However, the corrosion resistance was not able to be fully explained by the degree of the stress build-up in the oxide. In this study, Zircaloy-4 having a higher fraction of the

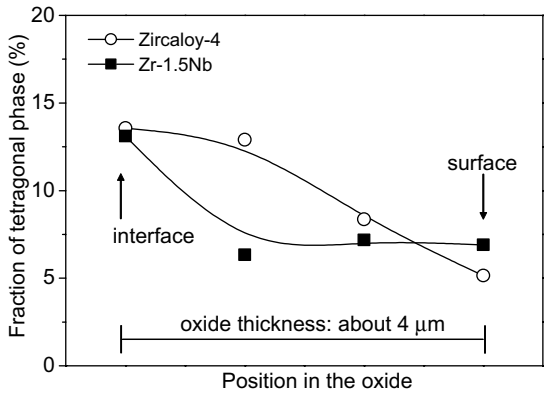

Fig. 8. Calculated fraction of the tetragonal phase as a function of the position in the oxide formed on Zircaloy-4 and Zr–1.5wt%Nb.

tetragonal phase, which could be attributed to the higher stress build-up in the oxide, showed an inferior corrosion resistance as compared to Zr–1.5Nb. This is consistent with the Petigny et al.'s result [27] showing that Zr–1NbO showed the higher corrosion rate in the oxidation test at 470 °C under 10^4 Pa of oxygen although the stress build-up near the metal/oxide interface was higher as compared to Zircaloy-4. Therefore, it is suggested that the difference of corrosion resistance between Zircaloy-4 and Zr–1.5Nb in this study was not able to be clarified solely by the tetragonal phase stability connected with the stress build-up.

3.4. Grain morphology of oxides

Grain morphology of the oxide is also considered to be an important factor controlling the corrosion kinetics since the corrosion of the Zr alloys is proceeded by oxygen diffusion through the oxide which is sensitive to the grain size of the oxide. In general, two types of grain morphology are formed during the corrosion process according to the many investigations using the TEM observation: the columnar and equiaxed grains. It has been reported that the columnar grain, which usually has a larger grain size than the equiaxed one, is more protective against the corrosion [9,10]. This is caused by the fact that grain boundary area which acts as a major diffusion path of the oxygen is smaller in the columnar grains than in the equiaxed ones.

In this investigation, the grain sizes of the tetragonal and monoclinic phases in the oxides were determined by the following equation.

$$D = 0.9\lambda/B\cos\theta, \tag{3}$$

where D is the grain size, B is the peak width after correction of the instrumental width, θ is the diffraction angle and λ is the wavelength of the synchrotron radiation.

The full width at half maximum (FWHM) of the peaks corresponding to the tetragonal and monoclinic phase was determined from the diffracted intensity against the two-theta shown in Figs. 5 and 7 to use as B in calculating the grain size of the tetragonal and monoclinic phase.

Figs. 9 and 10 show the variation of the calculated grain sizes of the tetragonal and monoclinic phase as a function of the position in the oxides formed on Zircaloy-4 and Zr–1.5Nb, respectively. The grain size of the monoclinic phase was calculated from the diffracted intensity peaks M($\bar{1}11$), M(111) and M(200) in Figs. 5 and 7, and the average of the calculated values were plotted together with the scatter band. The same procedure was applied to calculating the grain size of the tetragonal phase using the diffracted intensity peaks, T(101) and T(002) in Figs. 5 and 7. The grain size of the oxides calculated from the tetragonal peak was smaller than those from the monoclinic peaks in both alloys

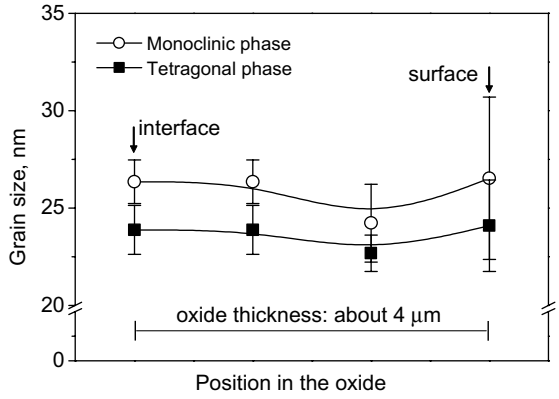

Fig. 9. Calculated grain sizes of the tetragonal and monoclinic phase as a function of the position in the oxide formed on Zircaloy-4.

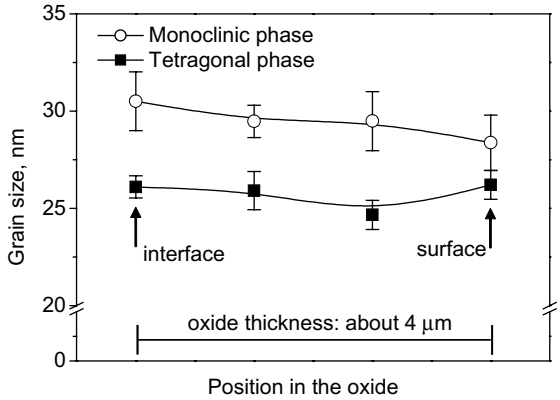

Fig. 10. Calculated grain sizes of the tetragonal and monoclinic phase as a function of the position in the oxide formed on Zr–1.5wt%Nb.

and did not greatly change with the distance from the metal/oxide interface. The calculated result also revealed that the grain size of the oxide was a little larger in Zr–1.5Nb than in Zircaloy-4.

It has been reported that the volume ratio of the equiaxed grain to the columnar one in Zr oxide increased when the weight gain after the first transition increased [6]. It was suggested that the grain boundary diffusion of the oxygen ion was accelerated by the transformation of the Zr oxide microstructure from large columnar grains to fine equiaxed ones. In addition, the equiaxed grains were dominantly observed around the precipitate which was incorporated into the oxide, which suggests that the transformation of the oxide microstructure might be caused dominantly by the oxidation of the intermetallic precipitates [6]. It was also proposed that the transformation of the oxide morphology of the

Nb-containing Zr alloys from the columnar grain to the equiaxed one was exceedingly accelerated when a precipitate larger than a specific size was incorporated into the oxide during the corrosion [28]. It is implied that the optimum corrosion resistance of the Nb-containing Zr alloys is achieved by maintaining a uniform distribution of the fine second phase particles [28]. In this study, a larger grain size in the oxide of Zr–1.5Nb seems to be attributed to the smaller size of β_{Nb} precipitate compared to the $Zr(Fe,Cr)_2$ in Zircaloy-4.

From the results obtained, it was found that Zr–1.5Nb showed a better corrosion resistance than Zircaloy-4 and the grain size of the tetragonal and monoclinic phase was a little larger in the oxide of Zr–1.5Nb regardless of the peaks used in the calculation. Many researchers have proposed that corrosion behavior is considerably related to the stability of the tetragonal phase in the protective oxide near the metal/oxide interface [8,17,18]. In this study, however, the tetragonal phase fraction at the interface was almost the same in both alloys, which implies that the tetragonal phase fraction cannot clarify the difference in the corrosion behaviors of Zircaloy-4 and Zr–1.5Nb. It seems reasonable to suppose that the superior corrosion resistance of Zr–1.5Nb to Zircaloy-4 was attributed to the larger grain size of the oxide in which the oxygen diffusion is expected to be lowered when compared to the smaller grain size. It could therefore be concluded that the grain size of the oxide is a more dominant factor controlling the corrosion resistance of the Zr alloys used in this study.

4. Conclusions

Microstructure, corrosion behavior and oxide properties of Zircaloy-4 and Zr–1.5Nb have been investigated to enhance the understanding of the relationship between the corrosion behavior and the oxide characteristics of the Zr alloys. Zr–1.5Nb alloy which had a fully-recrystallized structure with a fine distribution of β_{Nb} showed a better corrosion resistance than the stress-relieved Zircaloy-4 tube in 360 °C pure water up to 300 days. From the results of the microbeam X-ray diffraction using a synchrotron radiation, the fraction of the tetragonal phase in the oxide was found to have a maximum and almost the same value near the interface in both alloys and decreased when apart from the interface. The higher fraction of the tetragonal phase was maintained at a further distance from the interface in the oxide of Zircaloy-4 as compared to that of Zr–1.5Nb. Although the tetragonal phase in the oxide was more stable as a whole in Zircaloy-4, the corrosion resistance was shown to be better in Zr–1.5Nb. The stability of the tetragonal phase in the oxide was not thought to be able to clarify the difference in the corrosion behavior of the two alloys. From the calculation of the grain size from the diffracted intensity, it was found that the oxide of the Zr–1.5Nb had larger grains than that of Zircaloy-4 with the tetragonal phase being smaller than the monoclinic one. The grain size of the oxide was not greatly changed with the position in the oxide in both alloys. It seems reasonable to suppose that the superior corrosion resistance of Zr–1.5Nb was attributed to the larger grain size of the oxide in which the oxygen diffusion is expected to be lowered when compared to the smaller grain size of oxide on Zircaloy-4.

Acknowledgments

This work has been carried out under the nuclear R&D program by MOST in Korea. Experiments at PLS were supported in part by MOST and POSTECH.

References

[1] L.F. van Swam, F. Garzarolli, E. Steinberg, Proceedings of International Topical Meeting on LWR Fuel Performance, ANS, West Palm Beach, FL, 1994, p. 303.
[2] G.P. Sabol, G.R. Kilp, M.G. Balfour, E. Roberts, ASTM STP 1023 (1989) 227.
[3] J.P. Mardon, D. Charquet, J. Senevat, ASTM STP 1354 (2000) 505.
[4] A.M. Garde, S.R. Pati, M.A. Krammen, G.P. Smith, R.K. Endter, ASTM STP 1245 (1994) 760.
[5] D. Pecheur, F. Lefebvre, A.T. Motta, C. Lemaignan, D. Charquet, ASTM STP 1245 (1994) 687.
[6] H. Anada, B.J. Herb, K. Nomoto, S. Hagi, R.A. Graham, T. Kuroda, ASTM STP 1295 (1996) 74.
[7] F. Garzarolli, E. Steinberg, H.G. Weidinger, ASTM STP 1023 (1989) 202.
[8] J. Godlewski, ASTM STP 1245 (1994) 663.
[9] D. Pecheur, J. Godlewski, P. Billot, J. Thomazet, ASTM STP 1295 (1996) 94.
[10] F. Garzarolli, H. Seidel, R. Tricot, J.P. Gros, ASTM STP 1132 (1991) 395.
[11] A. Yilmazbayhan, A.T. Motta, R.J. Comstock, G.P. Sabol, B. Lai, Z. Cai, J. Nucl. Mater. 324 (2004) 6.
[12] K.T. Erwin, O. Delaire, A.T. Motta, Y.S. Chu, D.C. Mancini, R.C. Birtcher, J. Nucl. Mater. 294 (2001) 299.
[13] Y.H. Jeong, H.G. Kim, T.H. Kim, J. Nucl. Mater. 317 (2003) 1.
[14] G.P. Sabol, R.J. Comstock, R.A. Weiner, P. Larourer, R.N. Stanutz, ASTM STP 1245 (1994) 724.
[15] R.C. Garvie, P.S. Nicholson, J. Am. Ceram. Soc. 55 (1972) 303.
[16] P. Barberis, A. Frichet, J. Nucl. Mater. 273 (1999) 182.
[17] J. Godlewski, J.P. Gros, M. Lanbertin, J.F. Waider, H. Weidinger, ASTM STP 1132 (1991) 416.
[18] H.J. Beie, A. Mitwaslky, F. Gazarolli, H. Ruhmann, H.J. Sell, ASTM STP 1245 (1994) 615.
[19] P. Barberis, J. Nucl. Mater. 226 (1995) 34.

[20] E. Djurado, P. Bouvier, G. Lucazeau, J. Solid State Chem. 149 (2000) 399.
[21] P. Bouvier, G. Lucazeau, J. Phys. Chem. Solids 61 (2000) 569.
[22] R.C. Garvie, J. Phys. Chem. 69 (1965) 34.
[23] P. Li, I.W. Chen, J.E. Penner-Hahn, J. Am. Ceram. Soc. 77 (1994) 1281.
[24] D.J. Kim, J. Am. Ceram. Soc. 73 (1990) 115.
[25] J. Godlewski, P. Bouvier, G. Lucazeau, L. Fayette, ASTM STP 1354 (2000) 877.
[26] M. Parise, O. Sicardy, G. Cailletaud, J. Nucl. Mater. 256 (1998) 35.
[27] N. Petigny, P. Barberis, C. Lemaignan, Ch. Valot, M. Lallemant, J. Nucl. Mater. 280 (2000) 318.
[28] J.Y. Park, Y.H. Jeong, Y.H. Jung, Metals Mater. Int. 7 (2001) 447.